# Acid–Base Strength and Acidochromism of Some Dimethylamino–Azinium Iodides. An Integrated Experimental and Theoretical Study

**ARTICLE** *in* THE JOURNAL OF PHYSICAL CHEMISTRY A · DECEMBER 2014

Impact Factor: 2.69 · DOI: 10.1021/jp510982h · Source: PubMed



**6 AUTHORS**, INCLUDING:

Benedetta Carlotti
Università degli Studi di Perugia
**40** PUBLICATIONS **296** CITATIONS
SEE PROFILE

Vincenzo Barone
Scuola Normale Superiore di Pisa
**773** PUBLICATIONS **44,695** CITATIONS
SEE PROFILE

Fausto Elisei
Università degli Studi di Perugia
**193** PUBLICATIONS **3,403** CITATIONS
SEE PROFILE

Anna Spalletti
Università degli Studi di Perugia
**102** PUBLICATIONS **1,203** CITATIONS
SEE PROFILE

THE JOURNAL OF PHYSICAL CHEMISTRY A

Article

pubs.acs.org/JPCA

# Acid–Base Strength and Acidochromism of Some Dimethylamino–Azinium Iodides. An Integrated Experimental and Theoretical Study

Enrico Benassi,*[,†] Benedetta Carlotti,[‡] Cosimo G. Fortuna,[§] Vincenzo Barone,[†] Fausto Elisei,[‡] and Anna Spalletti*[,‡]

[†]Scuola Normale Superiore, Piazza dei Cavalieri 7, 56126 Pisa, Italy

[‡]Department of Chemistry, Biology and Biotechnology and Centro di Eccellenza sui Materiali Innovativi Nanostrutturati (CEMIN), University of Perugia, via Elce di Sotto 8, 06123 Perugia, Italy

[§]Department of Chemical Sciences, University of Catania, viale Andrea Doria 6, 95125 Catania, Italy

Supporting Information

**ABSTRACT:** The effects of pH on the spectral properties of stilbazolium salts bearing dimethylamino substituents, namely, trans isomers of the iodides of the dipolar *E*-[2-(4-dimethylamino)styryl]-1-methylpyridinium, its branched quadrupolar analogue *E,E*-[2,6-di-(*p*-dimethylamino)styryl]-1-methylpyridinium, and three analogues, chosen to investigate the effects of the stronger quinolinium acceptor, the longer butadiene $\pi$ bridge, or both, were investigated through a joint experimental and computational approach. A noticeable acidochromism of the absorption spectra (interesting for applications) was observed, with the basic and protonated species giving intensely colored and transparent solutions, respectively. The acid–base equilibrium constants for the protonation of the dimethylamino group in the ground state ($pK_a$) were experimentally derived. Theoretical calculations according to the thermodynamic Born–Haber cycle provided $pK_a$ values in good agreement with the experimental values. The very low fluorescence yield did not allow a direct investigation of the changes in the acid–base properties in the excited state ($pK_a^*$) by fluorimetric titrations. Their values were derived by quantum-mechanical calculations and estimated experimentally on the basis of the Förster cycle.


## 1. INTRODUCTION

Stilbazolium salts bearing dimethylamino substituents are of interest as fluorescent sensors[1] because the introduction of the dialkylamino group generally implies significant changes in the emission quantum yield, often accompanied by changes in the yield of the competitive trans → cis photoisomerisation.[2] Additionally, these compounds have a push–pull character bearing a strong electron acceptor, the pyridinium group (A), and a strong donor, the dimethylanilino group (D); therefore, they can show a marked solvatochromism coupled to nonnegligible nonlinear optical (NLO) properties.[3,4]

In this work, we aim to investigate the effects of protonation of the dimethylamino group on the spectral and photophysical properties of two stilbazolium salts and related molecules (Scheme 1), through a joint experimental (absorption and emission techniques) and computational [density functional theory (DFT)/polarizable continuum model (PCM)] approach. The investigated systems are the trans (*E*) isomers of the iodides of the dipolar *E*-[2-(4-dimethylamino)styryl]-1-methylpyridinium (**1**, the reference compound), its branched quadrupolar analogue *E,E*-[2,6-di-(*p*-dimethylamino)styryl]-1-methylpyridinium (**2**), and three analogues, chosen to investigate the effects of the stronger quinolinium acceptor (**3**), the longer butadiene $\pi$ bridge (**4**), or both (**5**). The negative solvatochromism of compound **1** (commonly referred to as *o*-DASPMI) was previously studied[5−10] by experimental spectroscopic measurements (stationary and ultrafast techniques) and theoretical DFT calculations. With reference to the latter, the dipole moment was computed for the ground ($\mu_g$) and excited Franck–Condon (FC) ($\mu_{FC}$) states and for the relaxed state ($\mu_{TICT}$, TICT stands for twisted intramolecular charge transfer) formed after completion of the charge movement in the excited $S_1$ state in solvents of different polarities.[10] A relatively high value [$\mu_g$ = 6.9 in dichloromethane (DCM)] was found for the dipole moment of the most stable conformer in the ground state, due to the positive charge largely localized in the pyridinium group, as indicated by the computed Mulliken charges. The molecular orbitals and the charge densities showed the charge-transfer (CT) character of the transition under light absorption, leading to electron transfer toward the pyridinium group, which reduces the polar character of the FC excited state ($\mu_{FC}$ = 3.3 D for **1** in DCM). The dipole moment component along the principal molecular axis was shown to change direction upon excitation.[10]

After the fast vibronic relaxation expected for these flexible molecules, the so-called "locally excited" (LE) state (still planar

**Received:** November 2, 2014
**Revised:** December 18, 2014

  

DOI: 10.1021/jp510982h
J. Phys. Chem. A XXXX, XXX, XXX−XXX

**Scheme 1. Molecular Structures of the Cations Investigated**

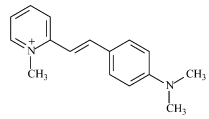

*E*–2–(4–dimethylaminostyryl), 1–methylpyridinium (**1**)

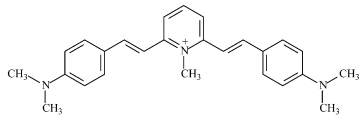

*E,E*–2,6–bis(4–dimethylaminostyryl), 1–methylpyridinium (**2**)

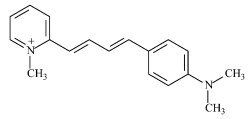

*E*–2–[4–(4–dimethylaminophenyl)–1,3–butadienyl)], 1–methylpyridinium (**3**)

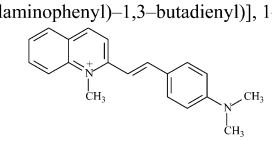

*E*–2–(4–dimethylaminostyryl), 1–methylquinolinium (**4**)

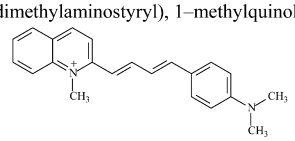

*E*–2–[4–(4–dimethylaminophenyl)–1,3–butadienyl)], 1–methylquinolinium (**5**)

but less polar than the ground state) undergoes further ICT accompanied by twisting of one of the side groups around one of the single bonds with the ethenic bridge. Our most recent calculations showed that, in the relaxed state of **1**, the twisting of the methylpiridinium group favors a back shift of the positive charge toward the pyridinium group. Correspondingly, the total dipole moment of the relaxed $S_1$ state increases and returns to the same direction as the ground state with a value ($\mu_{TICT}$) slightly higher than $\mu_g$ because the TICT state ensures better localization of the positive charge with respect to the planar ground state.[10] The TICT structure of $S_1$, mainly in polar solvents, was found to be in agreement with the fast deactivation through internal conversion (IC) and definitively confirmed by stationary and ultrafast measurements in viscous solvents (i.e., methanol/glycerol mixtures) that cause the increase of the fluorescence quantum yield and time constants hindering the torsional movements.[10]

Three components were generally found by ultrafast transient absorption measurements for **1** and assigned to the combined effects of solvent reorientation and further changes in the electronic distribution during the lifetime of the excited state. This led to an understanding of the different behaviors in less-polar solvents, where the charge movement is slower than the solvent reorientation, and in polar solvents, where the situation is inverted.[10]

Recently,[11] we reported that, after photoexcitation, compound **2** (previously studied in much less detail[12−14]), which can be rationalized as a symmetric charge quadrupole, shows a symmetry breaking in the first singlet excited state that is responsible for its enhanced CT character and NLO properties. Also, compound **3**[15−17] and particularly compounds **4** and **5** have been little investigated. For the latter, only some synthetic information is available in the literature.[11] For all five compounds investigated, no information on the protonation constants is available to the best of our knowledge.

As described for **1**,[10] the hypsochromic shift of the absorption of these compounds on going from nonpolar to polar solvents is clear but relatively modest, thus leading to a moderate solvatochromism.[10,11,18] It should also be noted that protic and hydrogen-bonding solvents, hampering the charge displacements, can also contribute to the blue shift of the absorption spectrum. Therefore, it is expected that the acid−base properties of the dimethylamino group, not investigated so far for these compounds, should produce interesting spectral changes (acidochromism). The effects of pH on the spectra of compounds **1** and **2** were discussed in a previous work, but the acid−base titration was not reported.[13] The main aim of this work is to study the effects of pH on the spectral properties of compounds **1**−**5** and to derive their acid−base equilibrium constants for the protonation of the dimethylamino group both in the ground state ($pK_a$) and in the excited state ($pK_a^*$) through an integrated experimental and computational approach. The very low fluorescence yield and the absence of a clear sign of re-equilibration in $S_1$ did not allow a direct investigation of the changes in the acid−base properties in the excited state ($pK_a^*$), performing fluorimetric titrations that were then derived by quantum-mechanical calculations and estimated experimentally on the basis of the Förster cycle (vide infra).

## 2. MATERIALS AND METHODS

**2.1. Materials.** The investigated compounds **1**−**5** of Scheme 1 were synthesized as iodide salts at the Catania Laboratory (Catania, Italy) in previous works[10,11,18−20] following the procedure described elsewhere.[21] The acid−base properties were measured in aqueous solutions at different pH values using Britton buffers in the 2−10 pH range and dilute $HClO_4$ solutions in the acidic region.

**2.2. Photophysical Measurements.** A Perkin-Elmer Lambda 800 spectrophotometer and a Spex Fluorolog-2 F112AI spectrofluorimeter were used for absorption and emission measurements, respectively. Dilute solutions (absorbance < 0.1 at the excitation wavelength, $\lambda_{exc}$) were used for fluorimetric measurements. The fluorescence quantum yields ($\phi_F$) were determined at $\lambda_{exc}$ corresponding to the maximum of the first absorption band ($\lambda_{max}$). 9,10-Diphenylanthracene in cyclohexane was used as the fluorimetric standard ($\phi_F$ = 0.90 in de-aerated solvent[22]).

A detailed description of the experimental setup for ultrafast spectroscopic and kinetic measurements has already been reported.[23,24] The 400-nm excitation pulses of ca. 60 fs were generated by an amplified Ti:sapphire laser system (Spectra Physics, Mountain View, CA). The transient absorption setup (Helios, Ultrafast Systems) is characterized by a temporal resolution of ca. 150 fs and a spectral resolution of 1.5 nm. All measurements were carried out under magic angle conditions in a 2-mm cell at an absorbance of about 0.1−0.3 at 400 nm. The solution was stirred during the experiments to avoid photoproduct interferences. Transient absorption data were analyzed using Surface Xplorer PRO (Ultrafast Systems) software where it was possible to perform singular value decomposition[25,26] of the three-dimensional surface into principal components (spectra and kinetics) and to perform global analysis [giving lifetimes and decay associated spectra (DAS) of the detected transients][27] with a number of components determined on the basis of best fitting procedure. Only consecutive first-order reactions were considered.



DOI: 10.1021/jp510982h
J. Phys. Chem. A XXXX, XXX, XXX−XXX

**2.3. Computational Details.** The species sketched in Scheme 1 and their respective singly protonated forms were initially optimized in the gas phase by density functional theory (DFT).[28−31] The 6-31+G(d) basis set and Handy and co-workers' long-range corrected version of the Becke three-parameter Lee−Yang−Parr (B3LYP) exchange−correlation functional[32] using the Coulomb-attenuating method (CAM−B3LYP)[33] were employed. The optimized geometries were then submitted to frequency calculations. From this, we obtained the $G_{(gas)}$ values. The absence of imaginary frequencies confirmed that the structures were true minima at their respective levels of calculation. To calculate $\Delta G_{(s)}$ values, the geometries were then reoptimized in water at the same levels of theory including the integral equation formalism polarizable continuum model (IEF-PCM)[34−36] with radii and nonelectrostatic terms for Truhlar and co-workers' SMD solvation model.[37] The properties of the first five singlet excited electronic states and the first five triplet excited electronic states, the wave functions, and the electronic spectra were investigated by time-dependent DFT (TD-DFT). The $S_1$ state geometry was optimized both in vacuo and in implicit solvents. We also verified the effect of the presence of one explicit water molecule close to the amino group in addition to the continuum model. All computations were performed by employing the Gaussian 09 package.[38]

## 3. METHODOLOGIES

**3.1. Computational Evaluation of p$K_a$ and p$K_a^*$.** The computational estimation of both p$K_a$ and p$K_a^*$ requires the determination of the variation in Gibbs free energy, following the Born−Haber thermodynamic cycle

$$\begin{array}{ccccc} HA_{(gas)} & \overset{\Delta G_{(gas)}}{\rightleftharpoons} & H^+_{(gas)} & + & A^-_{(gas)} \\ \Updownarrow \Delta G_s(HA) & & \Updownarrow \Delta G_s(H^+) & & \Updownarrow \Delta G_s(A^-) \\ HA_{(aq)} & \overset{\Delta G_{(aq)}}{\rightleftharpoons} & H^+_{(aq)} & + & A^-_{(aq)} \end{array}$$

In our case, the species involved are the cations reported in Scheme 1 and their respective singly protonated forms, where the proton addition occurs at the dimethylamino group. Using the Born−Haber cycle in the preceding equation, we calculated the absolute p$K_a$ and p$K_a^*$ values for the acid−base couple in its lowest-energy gas-phase and aqueous conformations in the electronic $S_0$ and $S_1$ states. Following well-tested approaches, all free energies were obtained from DFT/PCM or TD-DFT/PCM computations, except for those of the proton, which involves a number of difficulties.[39−44] To avoid these problems, the current practice is to compute relative p$K_a$ and p$K_a^*$ values referred to an internal standard (here, for instance, compound **1**). As discussed later in section 4.2, we preferred to use the most recent experimental values for the proton and to compute absolute p$K_a$ and p$K_a^*$ values, which can be directly compared to experiments. Furthermore, we computed vibrational frequencies both in vacuo and in solution, thus relaxing the standard approximation (e.g., ref 48) of negligible solvatochromic shifts in frequencies.

p$K_a^*$ values were also computed using Förster−Weller cycles, focusing on the equilibrium/nonequilibrium situations, as well as on the possible role of explicit water molecules. Houari et al.[48] recently concluded that the use of nonequilibrium regimes in continuum solvent approaches[35,49,50] yields better results, because the Förster−Weller cycle approach is based on a fast process (absorption or fluorescence). Because computed absorption energies are usually closer to their experimental counterparts than emission energies, they should be preferred.

**3.2. Experimental Determination of the Photoacidity (p$K_a^*$).** From an experimental point of view, the direct measurement of p$K_a^*$ is performed by fluorimetric titration in the presence of fast partial or complete acid−base re-equilibration in the excited state, the latter being operative if it is fast enough to efficiently compete with the deactivation processes of the basic and acidic forms in $S_1$. In systems where no equilibration in the excited state is observed, an (approximate) estimation of p$K_a^*$ is employed by the indirect method, proposed by Förster[46] and Weller.[47] This method is experimentally easier than direct measurements, but introduces some approximations given that it is based on the knowledge of the p$K_a$ and the measurement of the absorption (and/or emission) transition energies of the acidic (HA) and basic ($A^-$) forms. Therefore, it does not account for the possible reversibility of the proton-transfer process and neglects the difference in the vibrational pattern between the electronic ground and excited states. The value of p$K_a^*$ can be found with the aid of Förster−Weller cycle

$$\Delta pK_a = pK_a - pK_a^* = \frac{N}{\ln 10\, RT}[\Delta E_{FEG}(HA) - \Delta E_{FEG}(A^-)] \approx \frac{Nh}{\ln 10\, RT}\Delta\bar{\nu}$$

where $N$ is Avogadro's number and $\Delta E_{FEG}$ is Förster energy gap, which is the free energy gap separating the ground state and the stable (thermodynamic) energy level of the species involved in the proton transfer in their electronic excited states.

The spectroscopic energy difference between the non-protonated and protonated forms was estimated from an analysis of both the normalized absorption and fluorescence spectra of the two species (as shown in Figure 1 for the compounds studied in the present work). The frequency value of the point of intersection of these spectra can be approximated as the 0−0 frequency (energy) gap between the ground state and the excited state. $\Delta E_{FEG}$ can also be evaluated from the experimental or theoretical values of the absorption and emission wavelengths (see section 4.2).

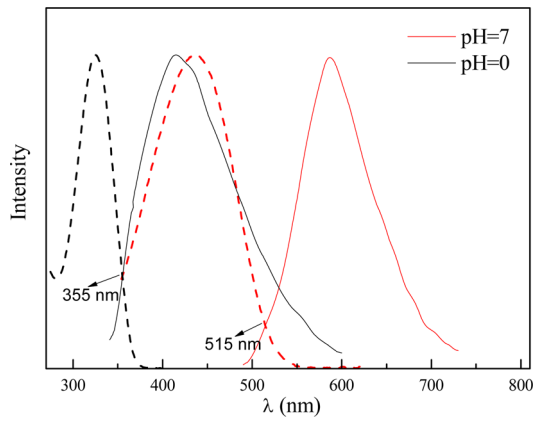


**Figure 1.** Normalized absorption (dashed line) and emission (solid line) spectra of the basic and monoprotonated species of **1** in buffered water (pH = 7) and $HClO_4$ (pH = 0).



DOI: 10.1021/jp510982h
J. Phys. Chem. A XXXX, XXX, XXX−XXX

Table 1. Spectral Properties ($\lambda$, $\varepsilon_{max}$, and Stokes shift $\Delta\nu$) of the Basic and Acidic Forms of Compounds 1−5 in Aqueous Solution

| | acidic pH = 0 | | | | basic pH = 5/7 | | | |
|---|---|---|---|---|---|---|---|---|
| compound | $\lambda^{ab}_{max}$ (nm) | $\varepsilon_{max}$ ($M^{-1}$ $s^{-1}$) | $\lambda^{em}_{max}$ (nm) | $\Delta\nu$ ($cm^{-1}$) | $\lambda^{ab}_{max}$ (nm) | $\varepsilon_{max}$ ($M^{-1}$ $s^{-1}$) | $\lambda^{em}_{max}$ (nm) | $\Delta\nu$ ($cm^{-1}$) |
| **1** | 325 | 28000 | 415 | 6670 | 437 | 25700 | 587 | 5850 |
| **2**[a] | 359 | 40720 | 446 | 5430 | 468 | 45500 | 590 | 4420 |
| **3** | 360 | 41540 | 448 | 5460 | 437 | 30720 | 678 | 8130 |
| **4** | 361 | 25020 | 425 | 4170 | 504 | 26550 | 640 | 4220 |
| **5**[b] | 395 | 31700 | 496 | 5160 | 503 | 25390 | 744 | 6440 |

[a]In water/EtOH (90:10,v/v). [b]In water/EtOH (95:5,v/v).

## 4. RESULTS AND DISCUSSION

**4.1. Spectral Properties.** As expected,[10,11,18] monocations **1**−**5** display negative solvatochromism, contrary to their less-polar neutral analogues bearing the pyridine group, which become more polar under excitation, causing ICT-induced positive solvatochromism (modest for the absorption spectra, but substantial for the emission spectra).[51−53] The monocation pyridinium analogues display opposite behavior because the dipole moment decreases upon excitation and a negative solvatochromism is operative, generally limited to the absorption spectra.[10,11,18]

The spectral properties of the five compounds investigated are very sensitive to the pH of the solution. The protonation of the dimethylanilino group introduces a second positive charge in the molecules that thus lose their push−pull character. The absorption and emission spectra of the acidic bications, bearing the protonated dimethylanilino and pyridinium groups, are strongly shifted toward the blue compared with the corresponding monocations (nonprotonated D moiety), thus inducing an interesting acidochromism.

The large differences in the spectral properties of the basic and protonated species allowed a spectrophotometric acid−base titration to be easily performed. The results will be described separately for each compound.

Moreover, simple thermodynamics for the ground and excited states of the protonated molecule (AH) and its conjugated base (as discussed in section 2.2) predict that its excited state (AH*) is a stronger acid than the ground state when the absorption and emission spectra of the conjugated base are red-shifted with respect to those of the conjugated acid. Molecules that undergo significant coloration upon deprotonation, as observed in the case of the present compounds, should be powerful proton donors under irradiation, so-called photoacids or superphotoacids. The occurrence of excited-state proton transfer (ESPT) has been the subject of abundant literature (for reviews, see refs 54 and 55). More recently, ultrafast spectroscopy allowed the proton dissociation dynamics in $S_1$ to be followed.[56−58] The very nature of excited-state proton transfer (ESPT) allows the demands of instantaneous pH manipulation to be met through the control of photons rather than by chemical means. This could result in more facile pH management merely by controlling the excitation source.

The investigation of the protonated species by ultrafast transient absorption spectroscopy was performed only for compounds **3**−**5** owing to the minimal solubility and absorption spectral ranges of **1** and **2** that prevented solutions at pH = 0.5 from absorbing enough at 400 nm for spectra to be obtained. The results showed that no re-equilibration in the excited state is operative, in agreement with short-lived singlet excited states (see section 4.1.3) and fluorimetric measurements at different pH values.

The structural and electronic properties were also investigated by quantum-mechanical calculations. A comparison between the experimental and theoretical results is reported in section 4.2.

*4.1.1. Compound 1 (Pyridinium Derivative).* Figures 1 and S1 (Supporting Information) show the absorption and emission spectra of compounds **1** and **2**−**5**, respectively, bearing the neutral amino group at pH = 5/7 and the protonated amino group at pH = 0/$H_0$ = −4. Table 1 shows the spectral maxima ($\lambda^{ab}_{max}$ and $\lambda^{em}_{max}$) and absorption coefficients ($\varepsilon_{max}$) of the first band for the basic and acidic species of **1**, together with those of compounds **2**−**5**. The spectra of the acidic (dication) species are shifted toward the blue when compared with those bearing the nonprotonated dimethylanilino group (monocation), the shift of the absorption maximum ($\Delta\nu_{A-B}$) for **1** being around 7900 $cm^{-1}$ (Table 2). This shift is quite large and might be of interest for the acidochromic properties of this compound to be used as a fluorimetric probe.

Table 2. Acidochromism ($\Delta\nu_{A-B}$) of Compounds 1−5[a]

| compound | $\Delta\nu_{A-B}$ ($cm^{-1}$) |
|---|---|
| **1** | 7890 |
| **2** | 6490 |
| **3** | 4890 |
| **4** | 7860 |
| **5** | 5440 |

[a]Difference between $\lambda^{ab}_{max}$ of the acidic and basic forms.

The absorption titration, carried out at a wavelength corresponding to $\lambda^{ab}_{max}$ (435 nm) of the basic species of **1** (inset of Figure 2), gave a relatively low value of p$K_a$ (3.10, Table 3), indicating the difficulty of adding a proton to the dimethylamino group. This result can be compared with literature data, where a higher p$K_a$ value of 5.15 at 25 °C was reported for *N*,*N*-dimethylaniline (donor moiety of **1**).[59] This difference is expected because of the introduction of the acceptor group (i.e., methylpyridinium) in compound **1**, which increases the extent of charge separation and then the dissociation constant. Moreover, p$K_a$ values of 3.11[60] and 2.6[61] were reported for the positional isomer *p*-DASPMI; indeed, the latter lower value would better reflect that the para position favors further the effect of the ICT process.

Table 4 collects the emission quantum yields of the acidic and basic forms of **1**, together with those of the other four compounds. The basic form displays a rather low fluorescence quantum yield, on the order of 0.001 in buffered water at pH = 7. The negligible $\phi_F$ value remains practically unchanged in the protonated form.



DOI: 10.1021/jp510982h
J. Phys. Chem. A XXXX, XXX, XXX−XXX

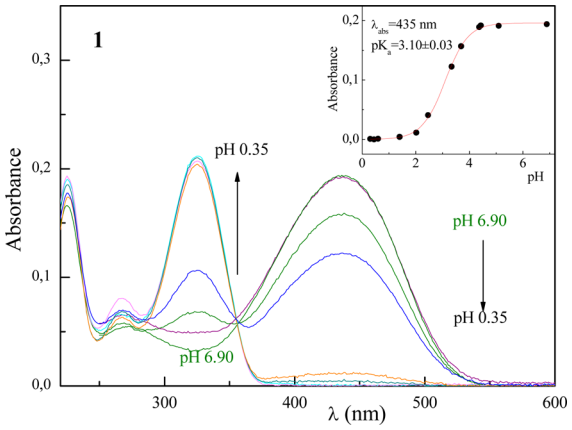


**Figure 2.** Absorption spectra of **1** as a function of pH. Inset: Titration curve at $\lambda_{max}$ of the nonprotonated species.

**Table 3. Measured Dissociation Constants of Compounds 1−5 in the Ground State and Predicted Values for the Excited State as Calculated by the Förster−Weller Cycle**

| compound | p$K_a$ | p$K_a^*$ |
|---|---|---|
| **1** | 3.10 | −15.2 |
| **2** | 2.86 | −9.0 |
| **3** | 3.12 | −8.8 |
| **4** | 1.97 | −10.0 |
| **5** | 2.63 | −13.1 |

**Table 4. Fluorescence Quantum Yields of the Acidic and Basic Forms of Compounds 1−5 in Aqueous Solutions**

| | $\phi_F$ | |
|---|---|---|
| compound | acidic (pH = $1/H_0$ = −1) | basic (pH = 5/7) |
| **1** | 0.001 | 0.001[a] |
| **2** | 0.02 | 0.0001[b] |
| **3** | 0.0004 | 0.005 |
| **4** | 0.002 | 0.0001 |
| **5** | 0.001 | 0.0007 |

[a]From ref 10. [b]From ref 11.

The very weak emission yields of both the monocation and dication of **1** (Table 4) prevented us from performing a complete fluorimetric titration. An attempt to obtain information on protonation in the excited state did not show signs of equilibration during the $S_1$ lifetime. However, the very short time constant (4.4 ps) obtained for the monocation by ultrafast spectroscopic measurements[10] and the observation that the dications are expected to have even shorter lifetimes (see Table 5, below) indicate that equilibrium between the two species is not achieved in the excited state because the proton transfer is too slow to compete with the deactivation of $S_1$, as also reported for *p*-DASPMI.[60]

Because the protonated species absorbs at higher energy than the basic one, an acidity increase in the excited state (p$K_a^*$ < p$K_a$) is expected upon application of the Förster−Weller cycle (see section 3.2). In fact, a p$K_a^*$ value of −15.2 was obtained using the 0,0 energy of the first transition estimated by the crossing of the normalized absorption and emission spectra of the two species in water at pH = 7 and 0 (see Figure 1). This value is rather more negative than that obtained for *p*-DASPMI (−13.5) by the same procedure.[61]

*4.1.2. Compound **2** (Branching Effect).* Figure S1 (Supporting Information) shows the spectra of the acidic and basic forms of **2**, which can be considered as a symmetric quadrupolar compound, where two donor groups are at the end of the molecule and the acceptor methylpyridinium group is the central unit (D−$\pi$−A−$\pi$−D). The absorption of the two-branch compound in the basic form is shifted to the red because of the longer $\pi$ system with respect to **1**. However, the shift is rather small (27 nm), indicating that the cross-conjugation of this meta compound makes the two styryl chromophores almost independent.[11] As expected for an angular (V-shaped) meta-substituted compound, where the two arms behave as almost separate chromophores, the extinction coefficient of **2** is almost twice that of **1** (45000 vs 25700 $M^{-1}$ $cm^{-1}$ in buffered water).[11]

Even here, the $S_0 \rightarrow S_1$ transition is expected to have a net CT character because of the charge transfer from the side aniline groups to the pyridinium core.[11]

The hypsochromic shift of the absorption spectrum of **2** upon protonation (Table 2) is shorter ($\Delta\nu_{A-B}$ = 6500 $cm^{-1}$) than that of **1** but still important for acidochromism. By acid−base titration of **2**, carried out by following the spectral evolution as a function of pH at 472 nm, the absorption maximum of the nonprotonated **2** (Figure S2, Supporting Information), a p$K_a$ value of 2.48 was measured for the first protonation constant, similar to that found for **1** (Table 3). The displacement of the absorption value at 355 nm at very negative $H_0$ function ($H_0$ = −4.5) from the plateau relative to the protonated **2** (inset on the right side of Figure S2, Supporting Information) is probably a sign of a further protonation (namely, that of the second dimethylamino group), which should lead to a biprotonated (tricationic) species, as reported for a positional isomer.[12]

At pH = 0, the fluorescence quantum yield increases by 2 orders of magnitude but remains rather weak (see Table 4). Because the protonated species absorbs at higher energy than the basic one, an acidity increase in the excited state was found even in this case by application of the Förster−Weller cycle (p$K_a^*$ = −9.0).

*4.1.3. Compound **3** (Chain Length Effect).* The extension of the $\pi$ core when the ethene is replaced by a butadiene bridge causes a spectral red shift with respect to **1**, particularly for fluorescence.[18] A larger delocalization in the excited state would be expected here, which should lower the LE energy, thus reducing the rate of TICT formation, owing to a higher barrier associated with the twisting ICT process. This is in agreement with the relatively longer lifetimes and less efficient intramolecular charge transfer observed in ultrafast absorption measurements for this compound.[18]

The titration was carried out monitoring the absorption spectrum at 450 nm (Figure S3) and led to a p$K_a$ similar to that of the ethene analogue **1**. On the contrary, its derived p$K_a^*$ was less negative than that of **1**, in agreement with the minor blue shift observed during protonation.

For compounds **3**−**5**, it was possible to perform ultrafast transient absorption measurements. The obtained results are collected in Table 5. In addition to a very short-lived (<1 ps) transient assignable to fast deactivation through solvent relaxation (solv) and a broad band that does not decay within the investigated time window (rest) and could be related to triplet or radical formation, the main transient observed and assigned to the poorly fluorescent $S_1$ showed fast deactivation (time constants of a few picoseconds, with the exception of **3** at


DOI: 10.1021/jp510982h
J. Phys. Chem. A XXXX, XXX, XXX−XXX

**Table 5. Kinetic Properties of 3−5 in Aqueous Buffered Solutions (Containing 10% v/v EtOH) Obtained by Ultrafast Transient Absorption Spectroscopy at $\lambda_{exc}$ = 400 nm**

| | $\tau$ (ps) | | | |
|---|---|---|---|---|
| pH | 3 | 4 | 5 | transient |
| 7 | 0.77 | 0.64 | 0.71 | solv |
| | 58 | 3.2 | 7.6 | $S_1$ |
| | | rest | rest | $T_1$ |
| 0.5 | 0.14 | <0.1 | 0.17 | solv |
| | 5.8 | 2.2 | 4.0 | $S_1$ |
| | rest | rest | rest | $T_1/R^{\bullet+}$ |

pH = 7; see Table 5). The lifetime of the basic species was found to decrease upon protonation (1 order of magnitude in the case of **3**), in agreement with the absence of re-equilibration in the excited state, which fails to effectively compete with the deactivation processes of $S_1$.

*4.1.4. Compound **4** (Quinolinium Effect).* The absorption/emission spectra of the acidic/basic forms of **4**, reported in Figure S1 and Table 1, display Stokes shifts of ~4200 $cm^{-1}$. *N*-Ethyl-2-styrylquinolinum iodides were investigated in two organic solvents and described as fluorescent probes that could find application in polymer chemistry to monitor the polymerization kinetics.[16] A spectral analysis in water was carried out in a recent work,[17] but the reported spectral maxima were quite different from those measured in our laboratory. Because the NMR analysis of compound **4** did not leave doubts about its structure, we consider our spectra quite reliable. The acidochromic shift of $\lambda^{ab}_{max}$ (7860 $cm^{-1}$) is rather similar to that of the pyridinium analogue.

Considering the stronger electron-withdrawing properties of the methylquinolinium group with respect to that of the methylpyridinium analogue, one expects that **4** should be a stronger acid than **1**. Indeed, the acid−base titration of **4** at the $\lambda^{ab}_{max}$ value of the basic form led to a p$K_a$ value of 1.97 (Figure S3 and Table 3).

*4.1.5. Compound **5** (Quinolinium and Chain Length Effects).* The presence of both the methylquinolinium group and the butadiene chain causes a further red shift of the absorption and emission spectra in less-polar solvents because of a larger $\pi$ delocalization.[18] In aqueous medium, the red shift is more significant for the protonated species (34 nm, if compared with **4**), leading to reduced acidochromism, higher only than that observed for **3** (see Figure S1 and Table 1).

Regarding acidity, compound **5** shows intermediate properties (p$K_a$) with respect to **3** and **4** and a very negative value for the acid−base equilibrium in the excited state (Table 3), second only to the p$K_a^*$ of the reference compound **1**.

Figure 3 shows the results of the femtosecond transient absorption measurements obtained for the basic and acidic forms of **5**. In fact, for this compound, the stronger absorption at the excitation wavelength of 400 nm for the protonated species allowed more intense and reliable transient signals to be obtained. In deionized water (Figure 3, left), the transient spectra show negative signals because of ground-state bleaching around 500 nm and stimulated emission (red shifting in time) around 700−750 nm, whereas a positive broad band of excited-state absorption is detected centered at 640 nm. Very different time-resolved spectra (confirming the lack of occurrence of acid−base re-equilibration in the excited state) were obtained during the ultrafast investigation of **5** at acidic pH (Figure 3, right). In this case, only positive transient signals were recorded in a spectral region significantly blue-shifted with respect to that of the basic species. In particular, an intense peak of absorption appears at 455 nm, together with a less intense band at 550 nm.

**4.2. Quantum Chemical Calculations.** *4.2.1. Protonation and Structures.* Before dealing with computed p$K_a$ values, let us spend a few words on the modifications of structural characteristics of the studied systems issuing from protonation, both in the ground and in the excited state, because some of

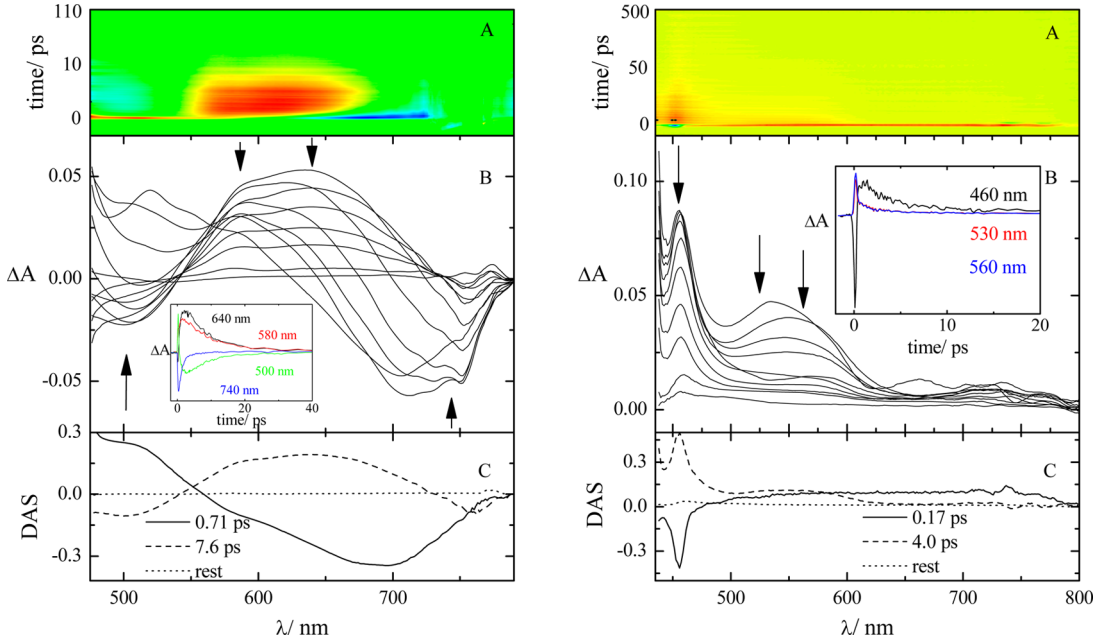


**Figure 3.** Pump−probe absorption spectroscopy of **5** in deionized water (left) and in buffered water at pH = 0.5 (right), containing a 10% v/v amount of EtOH: (A) Contour plot of the experimental data. (B) Time-resolved absorption spectra recorded at different delay times after the laser pulse. Insets: Decay kinetics recorded at meaningful wavelengths. (C) Amplitudes of the decay components obtained by SVD and global analysis.



DOI: 10.1021/jp510982h
J. Phys. Chem. A XXXX, XXX, XXX−XXX

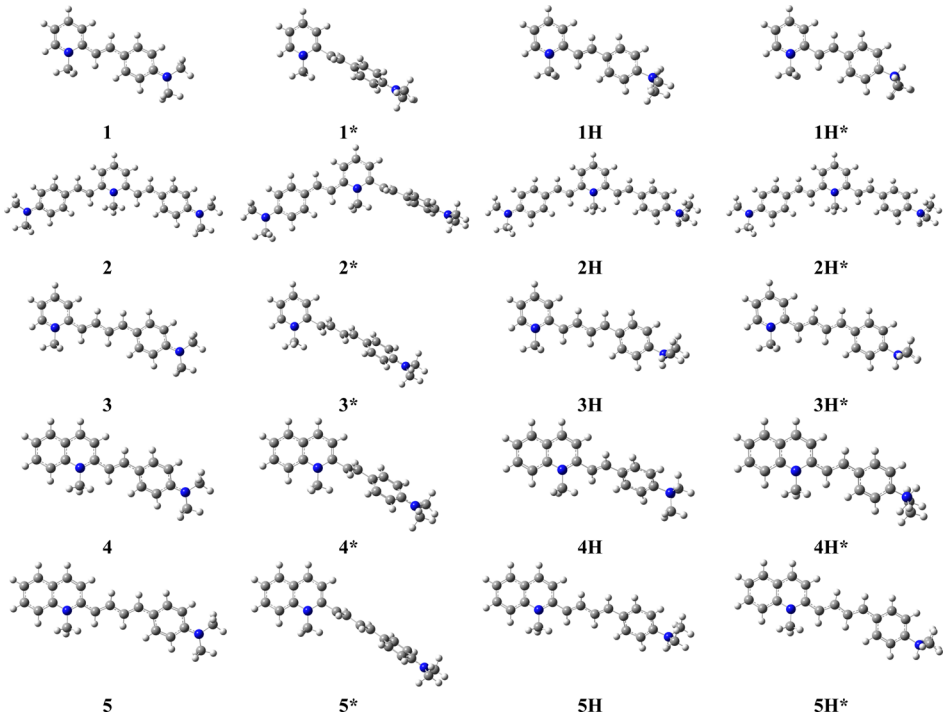


**Figure 4.** Optimized geometries of the nonprotonated (**3**–**5** from ref 18) and protonated forms of the investigated compounds, in the ground (*n*,*n*H) and excited (*n**,*n*H*) states, in implicit water (*n* = **1**–**5**).

**Table 6. Free Energy Differences (in kcal/mol) at 298.15 K and Comparison between Computed and Experimental Values of p$K_a$ and p$K_a^*$[a]**

| compound | $G_{(s)}(A^-) - G_{(s)}(HA)$ | $\Delta G_{(aq)}$ | $pK_a^{(theo)}$ | $pK_a^{(exp)}$ | $G_{(s)}(A^-*) - G_{(s)}(HA*)$ | $\Delta G^*_{(aq)}$ | $pK_a^{*(theo)}$ | $pK_a^{*(exp)}$ |
|---|---|---|---|---|---|---|---|---|
| **1** | 268.06 | 4.16 | 3.05 | 3.10 | 242.94 | −20.96 | −15.37 | −15.2 |
| **2** | 267. 73 | 3.83 | 2.81 | 2.86 | 250.78 | −13.12 | −9.62 | −9.0 |
| **3** | 268.11 | 4.21 | 3.09 | 3.12 | 250.84 | −13.06 | −9.58 | −8.8 |
| **4** | 266.53 | 2.63 | 1.93 | 1.97 | 247.93 | −15.97 | −11.72 | −10.0 |
| **5** | 267.62 | 3.72 | 2.73 | 2.71 | 244.40 | −19.50 | −14.30 | −13.1 |

[a]Value of $G_{(s)}(H^+)$ assumed to be −263.9 kcal/mol.

them can significantly tune the acid–base properties. There are two main alterations of the molecular geometry when the proton is added to the dimethylamino group: (1) When passing from $sp^2$ to $sp^3$ hybridization, the nitrogen atom of the dimethylamino group accepts the proton in a way that makes it coplanar with respect to the phenyl ring, forcing the two methyl groups, which are coplanar with respect to the phenyl ring in the nonprotonated chromophores, to now be above and below the plane of the ring. (2) The dihedral angle between the heteroatomic ring and the polyenic moiety is changed. Because the former structural modification is observed for all of the chromophores, it can be considered a *systematic change*. On the other hand, the latter change depends on the specific system and can thus be referred to as a *specific change*.

In Figure 4, the optimized geometries of the most stable conformers of the nonprotonated and protonated forms in $S_0$ and $S_1$ states in water are shown. It is evident that both protonation and photoexcitation cause changes to the geometry of the chromophores in water. For the nonprotonated one-branch systems, that is, all of the molecules except **2**, in vacuo, the planar (compounds **1** and **3**) or quasiplanar (compounds **4** and **5**) geometry of the ground state is retained when the excited state $S_1$ is populated. In water, a small distortion from coplanarity is observed for all compounds in the quasiplanar $S_0$ geometry, whereas the planarity of the systems is completely lost when $S_1$ is populated. In this case, the methylpyridinium/quinolinium group and the rest of the cation become nearly perpendicular. Upon protonation, the ground-state geometry tends to be slightly more distorted in water, with respect to the nonprotonated form, with a decreasing of the dihedral angle formed by the methylpyridinium/quinolinium group and the rest of the cation of about 10–15°. On the contrary, when the excited state is populated, the relaxed geometry of the protonated chromophores becomes almost flat (dihedral angle of 175–180°).

For the two-branch (nonprotonated) compound **2**, a symmetrical distortion of both the dimethylamino styryl portions with respect to the plane of the pyridinium ring for the ground electronic state, due to steric hindrance induced by the presence of the methyl group, has been reported,[11] in both low- and high-polarity solvents. In the former, the geometries of the ground and excited states are very close, whereas a symmetry breaking occurs in the first electronic excited state, that is, one of the two styryl moieties rotates with respect to the remaining portion of the cation.[11] When one of the two dimethylamino groups is protonated, the relaxed $S_1$ geometry does not undergo any symmetry breaking, remaining close to the $S_0$ geometry also in high-polarity solvents such as water.


DOI: 10.1021/jp510982h
J. Phys. Chem. A XXXX, XXX, XXX–XXX

Table 7. Comparison of Experimental and Theoretical Spectral Properties ($\lambda_{abs}$ and $\lambda_{em}$) and $\Delta pK_a$ values

| | experimental | | | | | | theoretical | | | | | |
|---|---|---|---|---|---|---|---|---|---|---|---|---|
| | nonprotonated | | protonated | | | | nonprotonated | | protonated | | | |
| compound | $\lambda_{abs}$ (nm) | $\lambda_{em}$ (nm) | $\lambda_{abs}$ (nm) | $\lambda_{em}$ (nm) | $\Delta pK_a$[a] | $\Delta pK_a$[b] | $\lambda_{abs}$ (nm) | $\lambda_{em}$ (nm) | $\lambda_{abs}$ (nm) | $\lambda_{em}$ (nm) | $\Delta pK_a$[a] | $\Delta pK_a$[c] |
| **1** | 438 | 589 | 325 | 415 | 15.78 | 18.30 | 440.39 | 586.16 | 327.92 | 413.54 | 15.63 | 18.42 |
| **2** | 464 | 590 | 359 | 446 | 12.34 | 11.86 | 466.20 | 587.95 | 360.57 | 444.01 | 12.36 | 12.43 |
| **3** | 438 | 680 | 362 | 500 | 10.57 | 11.92 | 440.37 | 678.63 | 363.96 | 498.72 | 10.57 | 12.67 |
| **4** | 498 | 625 | 362 | 420 | 16.09 | 11.97 | 498.65 | 628.01 | 363.02 | 424.25 | 15.87 | 13.65 |
| **5** | 503 | 752 | 394 | 497 | 12.91 | 15.81 | 504.45 | 755.03 | 395.15 | 501.06 | 12.78 | 17.03 |

[a]From the Förster–Weller cycle, i.e., $\Delta pK_a \approx [(Nh)/(\ln 10\ RT)]\Delta\bar{\nu}$. [b]From the Förster–Weller cycle, assuming $\Delta\bar{\nu} \equiv \Delta\bar{\nu}_{00}$, i.e., $\Delta pK_a \approx [(Nh)/(\ln 10\ RT)]\Delta\bar{\nu}_{00}$. [c]From the Born–Haber cycle, using data from Table 6.

*4.2.2. $pK_a$ and $pK_a^*$ Trends.* As mentioned in section 3.2, for homologous series of compounds, the current computational practice is to report relative $pK_a$ and $pK_a^*$ values referred to some internal standard. We instead decided to report the absolute values of $pK_a$ and $pK_a^*$ using the most trusted experimental values of $G_{(gas)}(H^+)$ (−6.28 kcal/mol[45]) and $\Delta G_{(sol)}(H^+)$ (−259.5 kcal/mol[39]) at $p$ = 1 atm and $T$ = 298.15 K, which lead to

$$G_{(s)}(H^+) \equiv G_{(gas)}(H^+) + \Delta G_{(sol)}(H^+) + RT\ \ln(24.46)$$
$$= -263.9\ \text{kcal/mol}$$

The notable agreement between computed and experimental values for compound **1** (3.05 vs 3.10 for $pK_a$ and −15.37 vs −15.2 for $pK_a^*$) point out the reliability of our computational approach and allow us to use absolute $pK_a$ values directly. Furthermore, we verified that, for the studied systems, the effects due to the inclusion of explicit solvent molecules are negligible (<1%).

For the whole series of investigated compounds, the computed $pK_a$ and $pK_a^*$ values (Table 6) and $\Delta pK_a = pK_a - pK_a^*$ values (Table 7) are in very good agreement with their experimental counterparts. A comparison between the experimental and computed values of $\Delta pK_a$ can be done at two levels (Table 7): (a) the $\Delta pK_a$ values obtained from the application of Förster–Weller cycle, using the absorption and emission energies, as obtained from the experiments and from quantum chemical calculations, and (b) the experimental $\Delta pK_a$ values obtained from the application of the Förster–Weller cycle assuming $\Delta\bar{\nu} \equiv \Delta\bar{\nu}_{00}$ with the computed $\Delta pK_a$ values obtained from the application of the Born–Haber cycle. Both approaches lead to good agreement between theory and experiment, confirming the strong photoacidity of the studied compounds. Linear regressions $x^{(exp)} = a_0 + a_1 x^{(theo)}$ lead to $a_0$ = (0.03 ± 0.10), $a_1$ = (1.00 ± 0.04) (adj $R^2$ = 0.99486) for $x$ = $pK_a$ and to $a_0$ = (1.34 ± 1.56), $a_1$ = (1.04 ± 0.13) (adj $R^2$ = 0.94314) for $x$ = $pK_a^*$. Although both trends can be considered satisfactory, a better correlation is obtained for the $pK_a$ values than for the $pK_a^*$ values because of the higher accuracy of the quantum chemical methods available for the description of the ground electronic state than the excited states.

An additional consideration can be made concerning the comparison between the Förster–Weller (FW) and Born–Haber (BH) approaches. Although use of the intersection of the first band of the absorption and emission experimental spectra ($\Delta\bar{\nu}_{00}$) for evaluating $\Delta pK_a$ through the Förster–Weller (kinetic) cycle gives results in agreement with those obtained theoretically through the Born–Haber (thermodynamic) cycle, the same cannot be said when we introduce the (experimental or theoretical) values of the wavenumbers of the absorption and emission maxima in the Förster–Weller cycle (Table 7). Following this approach, the experimental and theoretical values of $\Delta pK_a$(FW) are still in reciprocal agreement (this derives directly from the good matching found between experimental and computed transition energies, both in absorption and in emission), but deviate from the thermodynamic reference in a hardly rationalizable way [for **1**, **3**, and **5**, $\Delta pK_a$(FW) < $\Delta pK_a$(BH); for **2**, $\Delta pK_a$(FW) ≈ $\Delta pK_a$(BH); for **4** $\Delta pK_a$(FW) > $\Delta pK_a$(BH)]. Use of a thermodynamic approach is thus recommended.

As hinted in section 3.2, the thermodynamic cycle involved in the evaluation of $pK_a$ and $pK_a^*$ values is the same and involves, in principle, vibrational contributions both in the gas phase and in solution. We explicitly included those contributions without the simplifying assumption (used in all of the computational protocols suggested so far; e.g., ref 50) of negligible solvent effects on vibrational frequencies. Our results show that this improvement has non-negligible effects because, for instance, computations of $pK_a$(**1**) and $pK_a^*$(**1**) without the introduction of solvent shifts on frequencies leads to additional errors of ∼7.5% and ∼12.1%, respectively.

We now attempt to relate the change in the geometry due to the protonation and the photoexcitation to the $pK_a$ and $pK_a^*$ values. For the series of chromophores in this study, we systematically have $pK_a^* \ll pK_a$. This is due to the systematic change that we observed when the hybridization of the nitrogen atom of the dimethylamino group passes from $sp^2$ to $sp^3$ following the protonation. In the basic species, the dimethylamino group is involved in the p–$\pi$ conjugated system when the ground state is populated. After photoexcitation to $S_1$, the conjugation is different and is broken because of the protonation (acidic forms). This causes different stabilizations of the species with respect to the high-polarity surrounding solvent in the different states, and in particular, the stabilization is larger for the ground state than for the excited state.

As suggested in the previous sections, where the experimental data were presented and discussed, the different $pK_a$ and $pK_a^*$ values are related to the specific features of the chromophores and, therefore, can be ascribed to specific effects. In particular, if we consider the one-branch systems (in the case of **2**, the picture is more complicated), the variation of $pK_a$ in the two states ($\Delta pK_a$) correlates with the structural changes at the level of the dihedral angle defined by the heteroatomic ring and the polyenic moiety. With the aim of quantifying the change in this geometrical property, we define $\Delta\delta_{01}(X) \equiv \delta_{S_1}(X) - \delta_{S_0}(X)$ as the variation of the dihedral angle for species X due to the photoexcitation, $\Delta\delta_{HA-A^-}(S_n) \equiv \delta_{HA}(S_n) - \delta_{A^-}(S_n)$ as the variation of the dihedral angle between the acidic and basic forms in the state $S_n$ ($n$ = 0, 1), and finally $\Delta\Delta\delta \equiv$


DOI: 10.1021/jp510982h
J. Phys. Chem. A XXXX, XXX, XXX–XXX

$\Delta\delta_{01}(A^-) - \Delta\delta_{01}(HA) = \Delta\delta_{HA-A^-}(S_1) - \Delta\delta_{HA-A-}(S_0)$. When passing from $S_0$ to $S_1$, the dihedral angle decreases for all of the acidic forms and increases for all of the basic forms, that is, $\Delta\delta_{01}(HA) < 0$ and $\Delta\delta_{01}(A^-) > 0$, or equivalently, when the species are protonated (passing from basic to acidic form), the dihedral angle decreases for the ground state and increases for the excited state, that is, $\Delta\delta_{HA-A^-}(S_0) > 0$ and $\Delta\delta_{HA-A^-}(S_1) > 0$. Quantitatively, the variation of the dihedral angle is more significant for the basic forms than for the acidic ones, and it is more significant for $S_1$ than for $S_0$, and therefore, $\Delta\Delta\delta > 0$. In Figure 5, we show how the change in this geometrical property

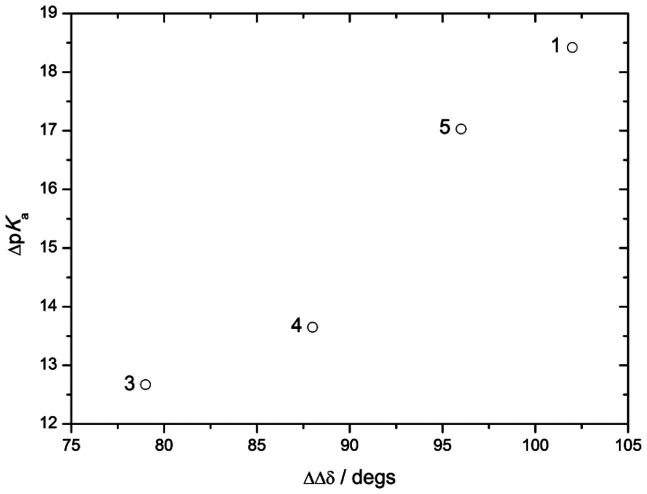


**Figure 5.** Plot of the variation of p$K_a$ in the two states ($\Delta pK_a$) as a function of the structural changes at level of the dihedral angle $\Delta\Delta\delta$ for the one-branch systems.

is related to the findings about the p$K_a$ and p$K_a^*$ values. If we apply a standard linear regression to the data, we obtain $\Delta pK_a = -0.2656\ \Delta\Delta\delta - 8.7903$ ($R^2 = 0.9454$).

## 5. CONCLUSIONS

In the present work, we aimed to study the acidity of some dimethylamino derivatives in the ground and excited states, through an integrated experimental and computational approach. The following conclusions can be drawn from the reported results:

The presence of the dimethylamino groups in the studied azinium iodides allowed interesting acid−base equilibria.

The compounds showed a noticeable acidochromism of their absorption spectra, with the basic and protonated species giving intensely colored and transparent solutions, respectively.

The protonation also implied a strong hypsochromic shift of the emission spectrum toward the blue, with the low fluorescence quantum yields showing an increase at acidic pH values, mainly in the case of the two-branch compound **2**.

The low p$K_a$ values (∼2−3 for all of the investigated compounds), derived by spectrophotometric titrations, indicated the nitrogen of the dimethylamino group to be hardly protonated. This fact could be related to the partial positive charge on the nitrogen present on the quinoid form that contributes to the description of these compounds in the ground state.

Theoretical calculation of the absolute p$K_a$ value for the acid−base couple in its lowest-energy gas-phase and aqueous conformations was also performed according to the thermodynamic Born−Haber cycle and provided p$K_a$ values in good agreement with the experimental ones.

The acid−base strength in the excited state (p$K_a^*$) was also estimated by both experimental and theoretical approaches. In the case of the experimental evaluation, the values were obtained by applying the indirect method, proposed by Förster and Weller, whereas from the computational point of view, the determination was acquired by applying both the Born−Haber thermodynamic cycle and the Förster−Weller scheme. Both approaches (experimental and computational) provided very negative values (in the range from −15 to −9), in good agreement with each other. The latter pointed to a strong potential photoacidity of these salts. However, no sign of acid−base re-equilibration in the excited state was found during the fluorimetric measurements and femtosecond transient spectroscopy performed in the case of compounds **3**−**5**, owing to the very fast decay dynamics of $S_1$.

In more general terms, the reliability of the computed results and the definition of a robust protocol available in a widely distributed computational code pave the route toward the accurate prediction and unbiased interpretation of the role played by different factors in tuning the acidity and photoacidity of large systems of current chemical and technological interest.

## ■ ASSOCIATED CONTENT

### Supporting Information

Additional information as noted in text. This material is available free of charge via the Internet at http://pubs.acs.org.

## ■ AUTHOR INFORMATION

### Corresponding Authors

*E-mail: enrico.benassi@sns.it.

*E-mail: anna.spalletti@unipg.it.

### Notes

The authors declare no competing financial interest.

## ■ ACKNOWLEDGMENTS

The authors thank the Italian "Ministero per l'Università e la Ricerca Scientifica e Tecnologica", MIUR (Rome, Italy) ([PRIN "Programmi di Ricerca di Interesse Nazionale" 2010−2011, 2010FM738P and FIRB "Futuro in Ricerca" 2013, RBFR13PSB6) and Regione Umbria (POR FSE 2007−2013, Risorse CIPE, Perugia, Italy) for funding. The authors thank also Prof. Ugo Mazzucato for stimulating discussions.

## ■ REFERENCES

(1) Fromherz, P.; Heilemann, A. Twisted Internal Charge Transfer in (Aminophenyl)Pyridinium. *J. Phys. Chem.* **1992**, *96*, 6864−6866 and references therein..

(2) Görner, H.; Gruen, H. Photophysical Properties of Quaternary Salts of 4-Dialkylamino-4′-azastilbenes and Their Quinolinium Analogues in Solution: IX. *J. Photochem.* **1985**, *28*, 329−350 and references therein..

(3) Strehmel, B.; Seifert, H.; Rettig, W. Photophysical Properties of Fluorescence Probes. 2. A Model of Multiple Fluorescence for Stilbazolium Dyes Studied by Global Analysis and Quantum Chemical Calculations. *J. Phys. Chem. B* **1997**, *101*, 2232−2243 and references therein..

(4) Sahoo, D.; Chakravorti, S. Spectra and Dynamics of an Ionic Styryl Dye in Reverse Micelles. *J. Photochem. Photobiol. A: Chem.* **2009**, *205*, 129−138 and references therein..



DOI: 10.1021/jp510982h
J. Phys. Chem. A XXXX, XXX, XXX−XXX

(5) Bingemann, D.; Ernsting, N. P. Femtosecond Solvation Dynamics Determining the Band Shape of Stimulated Emission from a Polar Styryl Dye. *J. Chem. Phys.* **1995**, *102*, 2691−2700.
(6) Jonkman, A. M.; Meulen, P. V. D.; Zhang, H.; Glasbeek, M. Subpicosecond Solvation Relaxation of DASPI in Polar Liquids. *Chem. Phys. Lett.* **1996**, *256*, 21−26.
(7) Van der Meer, M. J.; Zhang, H.; Rettig, W.; Glasbeek, M. Femto- and Picosecond Fluorescence Studies of Solvation and Non-Radiative Deactivation of Ionic Styryl Dyes in Liquid Solution. *Chem. Phys. Lett.* **2000**, *320*, 673−680.
(8) Glasbeek, M.; Zhang, H. Femtosecond Studies and Intramolecular Configurational Dynamics of Fluorophores in Liquid Solution. *Chem. Rev.* **2004**, *104*, 1929−1954 and references therein..
(9) Ramadass, R.; Bereiter−Hajn, J. Photophysical Properties of DASPMI as Revealed by Spectral Resolved Fluorescence Decays. *J. Phys. Chem. B* **2007**, *111*, 7681−7690.
(10) Carlotti, B.; Consiglio, G.; Elisei, F.; Fortuna, C. G.; Mazzucato, U.; Spalletti, A. Intramolecular Charge Transfer of Push−Pull Pyridinium Salts in the Singlet Manifold. *J. Phys. Chem. A* **2014**, *118*, 3580−3592.
(11) Carlotti, B.; Benassi, E.; Spalletti, A.; Fortuna, C. G.; Elisei, F.; Barone, V. Photoinduced Symmetry-Breaking Intramolecular Charge Transfer in a Quadrupolar Pyridinium Derivative. *Phys. Chem. Chem. Phys.* **2014**, *16*, 13984−13994.
(12) Matsui, M.; Kawamura, S.; Shibata, K.; Muramatsu, H. Synthesis and Characterization of Mono-, Bis-, and Trissubstituted Pyridinium and Pyrylium Dyes. *Bull. Chem. Soc. Jpn.* **1992**, *65*, 71−74.
(13) Wang, H.; Helgeson, R.; Ma, B.; Wudl, F. Synthesis and Optical Properties of Cross-Conjugated Bis(dimethylaminophenyl)-pyridylvinylene Derivatives. *J. Org. Chem.* **2000**, *65*, 5862−5867.
(14) Xu, X.; Qiu, W.; Zhou, Q.; Tang, J.; Yang, F.; Sun, Z.; Audebert, P. Nonlinear Optical Absorption Properties of Two Multisubstituted *p*-Dimethylaminophenylethenyl Pyridiniums. *J. Phys. Chem. B* **2008**, *12*, 4913−4917.
(15) Bahner, C. T.; Pace, E. S.; Prevost, R. Quaternary Salts of Styryl Pyridines and Quinolines. *J. Am. Chem. Soc.* **1951**, *73*, 3407−3408.
(16) Bajorek, A.; Kabatc, J.; Pączkowski, J. Novel *N*-Ethyl-2-styrylquinolinum Iodides as Fluorophores for Monitoring of Polymerization Process, Part I. *Dyes Pigm.* **2009**, *82*, 372−378.
(17) Sahoo, D.; Bhattacharya, P.; Chakravorti, S. Spectral Signature of 2-[4-(Dimethylamino)styryl]-1-methylquinolinium Iodide: A Case of Negative Solvatochromism in Water. *J. Phys. Chem. B* **2011**, *15*, 10983−10989.
(18) Carlotti, B.; Benassi, E.; Barone, V.; Consiglio, G.; Elisei, F.; Mazzoli, A.; Spalletti, A. Effect of the $\pi$-Bridge and the Acceptor on the Intramolecular Charge Transfer in Push−Pull Cationic Chromophores: A Joint Ultrafast Spectroscopic and TD-DFT Computational Study. *ChemPhysChem*, manuscript submitted.
(19) Fortuna, C. G.; Forte, G.; Pittala, V.; Giuffrida, A.; Consiglio, G. Could 2,6-bis((*E*)-2-(furan-2-yl)vinyl)-1-methylpyridinium iodide and analog compounds intercalate DNA? A first principle prediction based on structural and electronic properties. *Comput. Theor. Chem.* **2012**, *985*, 8−13.
(20) Barresi, V.; Bonaccorso, C.; Consiglio, G.; Goracci, L.; Musso, N.; Musumarra, G.; Satriano, C.; Fortuna, C. G. Modeling, design and synthesis of new heteroaryl ethylenes active against the MCF-7 breast cancer cell-line. *Mol. BioSyst.* **2013**, *9*, 2426−2429.
(21) Fortuna, C.; Barresi, V.; Bonaccorso, C.; Consiglio, G.; Failla, S.; Trovato-Salinaro, A.; Musumarra, G. Design, synthesis and in vitro antitumour activity of new heteroaryl ethylenes. *Eur. J. Med. Chem.* **2012**, *47*, 221−227.
(22) Bartocci, G.; Masetti, F.; Mazzucato, U.; Spalletti, A.; Baraldi, I.; Momicchioli, F. Photophysical and Theoretical Studies of Photoisomerism and Rotamerism of *trans*-Styrylphenanthrenes. *J. Phys. Chem.* **1987**, *91*, 4733−4743.
(23) Carlotti, B.; Fuoco, D.; Elisei, F. Fast and ultrafast spectroscopic investigation of tetracycline derivatives in organic and aqueous media. *Phys. Chem. Chem. Phys.* **2010**, *12*, 15580−15591.
(24) Del Giacco, T.; Carlotti, B.; Barbafina, A.; De Solis, S.; Elisei, F. Steady-state and timeresolved investigations of a crown thioether conjugated with methylacridinium and its complexes with metal ions. *Phys. Chem. Chem. Phys.* **2011**, *13*, 2188−2195.
(25) Golub, G. H.; Loan, C. F. V. *Matrix Computations*, 2nd ed.; Johns Hopkins University Press: Baltimore, MD, 1989.
(26) Strang, G. *Introduction to Linear Algebra*; Wellesley Cambridge Press: Wellesley, MA, 1998.
(27) Van Stokkum, I. H. M.; Larsen, D. S.; Van Grondelle, R. Global and Target Analysis of Time-Resolved Spectra. *Biochim. Biophys. Acta* **2004**, *1657*, 82−104.
(28) Hohenberg, P.; Kohn, W. Inhomogeneous Electron Gas. *Phys. Rev.* **1964**, *136*, B864−B871.
(29) Kohn, W.; Sham, L. J. Self-Consistent Equations Including Exchange and Correlation Effects. *Phys. Rev.* **1965**, *140*, A1133−A1138.
(30) Salahub, D. R., Zerner, M. C., Eds. *The Challenge of d and f Electrons: Theory and Computation*; ACS Symposium Series; American Chemical Society: Washington, D.C., 1989; Vol. *394*.
(31) Parr, R. G.; Yang, W. *Density-Functional Theory of Atoms and Molecules*; Oxford University Press: Oxford, U.K., 1989.
(32) Becke, A. D. Density-functional thermochemistry. III. The role of exact exchange. *J. Chem. Phys.* **1993**, *98*, 5648−5652.
(33) Yanai, T.; Tew, D.; Handy, N. A new hybrid exchange−correlation functional using the Coulomb-attenuating method (CAM-B3LYP). *Chem. Phys. Lett.* **2004**, *393*, 51−57.
(34) Tomasi, J.; Mennucci, B.; Cances, E. The IEF version of the PCM solvation method: An overview of a new method addressed to study molecular solutes at the QM ab initio level. *J. Mol. Struct. (THEOCHEM)* **1999**, *464*, 211−226.
(35) Tomasi, J.; Mennucci, B.; Cammi, R. Quantum Mechanical Continuum Solvation Models. *Chem. Rev.* **2005**, *105*, 2999−3093.
(36) Scalmani, G.; Frisch, M. J. Continuous surface charge polarizable continuum models of solvation. I. General formalism. *J. Chem. Phys.* **2010**, *132*, 114110.
(37) Marenich, A. V.; Cramer, C. J.; Truhlar, D. G. Universal Solvation Model Based on Solute Electron Density and on a Continuum Model of the Solvent Defined by the Bulk Dielectric Constant and Atomic Surface Tensions. *J. Phys. Chem. B* **2009**, *113*, 6378−6396.
(38) Frisch, M. J.; Trucks, G. W.; Schlegel, H. B.; Scuseria, G. E.; Robb, M. A.; Cheeseman, J. R.; Scalmani, G.; Barone, V.; Mennucci, B.; Petersson, G. A.; Nakatsuji, H.; Caricato, M.; Li, X.; Hratchian, H. P.; Izmaylov, A. F.; Bloino, J.; Zheng, G.; Sonnenberg, J. L.; Hada, M.; Ehara, M.; Toyota, K.; Fukuda, R.; Hasegawa, J.; Ishida, M.; Nakajima, T.; Honda, Y.; Kitao, O.; Nakai, H.; Vreven, T.; Montgomery, J. A., Jr.; Peralta, J. E.; Ogliaro, F.; Bearpark, M.; Heyd, J. J.; Brothers, E.; Kudin, K. N.; Staroverov, V. N.; Keith, T.; Kobayashi, R.; Normand, J.; Raghavachari, K.; Rendell, A.; Burant, J. C.; Iyengar, S. S.; Tomasi, J.; Cossi, M.; Rega, N.; Millam, J. M.; Klene, M.; Knox, J. E.; Cross, J. B.; Bakken, V.; Adamo, C.; Jaramillo, J.; Gomperts, R.; Stratmann, R. E.; Yazyev, O.; Austin, A. J.; Cammi, R.; Pomelli, C.; Ochterski, J. W.; Martin, R. L.; Morokuma, K.; Zakrzewski, V. G.; Voth, G. A.; Salvador, P.; Dannenberg, J. J.; Dapprich, S.; Daniels, A. D.; Farkas, Ö.; Foresman, J. B.; Ortiz, J. V.; Cioslowski, J.; Fox, D. J. *Gaussian 09*, revision D.01; Gaussian, Inc.: Wallingford, CT, 2009.
(39) Lim, C.; Bashford, D.; Karplus, M. Absolute pKa calculations with continuum dielectric methods. *J. Phys. Chem.* **1991**, *95*, 5610−5620.
(40) Tissandier, M. D.; Cowen, K. A.; Feng, W. Y.; Gundlach, E.; Cohen, M. H.; Earhart, A. D.; Coe, J. V.; Tuttle, T. R., Jr. The Proton's Absolute Aqueous Enthalpy and Gibbs Free Energy of Solvation from Cluster-Ion Solvation Data. *J. Phys. Chem. A* **1998**, *102*, 7787−7794.
(41) Tawa, G. J.; Topol, I. A.; Burt, S. K.; Caldwell, R. A.; Rashin, A. A. Calculation of the aqueous solvation free energy of the proton. *J. Chem. Phys.* **1998**, *109*, 4852−4863.
(42) Mejias, J. A.; Lago, S. Calculation of the absolute hydration enthalpy and free energy of $H^+$ and $OH^-$. *J. Chem. Phys.* **2000**, *113*, 7306−7316.


DOI: 10.1021/jp510982h
*J. Phys. Chem. A* XXXX, XXX, XXX−XXX

(43) Zhan, C. G.; Dixon, D. A. Absolute Hydration Free Energy of the Proton from First-Principles Electronic Structure Calculations. *J. Phys. Chem. A* **2001**, *105*, 11534−11540.
(44) Hwang, S.; Chung, D. S. Calculation of the Solvation Free Energy of the Proton in Methanol. *Bull. Korean Chem. Soc.* **2005**, *26*, 589−593.
(45) Rosenbaum, E. J. *Physical Chemistry*; Appleton-Century-Crofts: New York, 1970; p 351.
(46) (a) Förster, Th. Fluoreszenzspektrum und Wasserstoffionenkonzentration. *Naturwissenschaften* **1949**, *36*, 186−187. (b) Förster, Th. Die pH-Abhangigkeit der Fluoreszenz von Naphthalinderivaten. *Z. Elektrochem. Angew. Phys. Chem.* **1950**, *42*, 531−535.
(47) (a) Weller, A. Allgemeine Basenkatalyse bei der elektrolytischen Dissoziation angeregter Naphthole. *Z. Elektrochem. Angew. Phys. Chem.* **1954**, *58*, 849−853. (b) Urban, W.; Weller, A. Fluoreszenzuntersuchungen zum Mechanismus protolytischer Reaktionen in nichtwasrigen Medien I. Die Dissoziationsreaktion starker Sauren. *Ber. Bunsen−Ges. Phys. Chem.* **1958**, *67*, 787−791. (c) Weller, A. Outer and inner mechanism of reactions of excited molecules. *Discuss. Faraday Soc.* **1959**, *27*, 28−33. (d) Weller, A. Fast reactions of excited molecules. *Prog. React. Kinet.* **1961**, *1*, 187−214.
(48) Houari, Y.; Jacquemin, D.; Laurent, A. D. Methodological Keys for Accurate $pK_a^*$ Simulations. *Phys. Chem. Chem. Phys.* **2013**, *15*, 11875−11882.
(49) Caricato, M.; Mennucci, B.; Tomasi, J.; Ingrosso, F.; Cammi, R.; Corni, S.; Scalmani, G. Formation and relaxation of excited states in solution: A new time dependent polarizable continuum model based on time dependent density functional theory. *J. Chem. Phys.* **2006**, *124*, 124520.
(50) Improta, R.; Barone, V.; Santoro, F. Ab Initio Calculations of Absorption Spectra of Large Molecules in Solution: Coumarin C153. *Angew. Chem., Int. Ed.* **2007**, *46*, 405−408.
(51) Bruni, S.; Cariati, E.; Cariati, F.; Porta, F. A.; Quici, S.; Roberto, D. Determination of the Quadratic Hyperpolarizability of *trans*-4-[4-(Dimethylamino)styryl]pyridine and 5-Dimethylamino-1,10-phenanthroline from Solvatochromism of Absorption and Fluorescence Spectra: A Comparison with the Electric-Field-Induced Second-Harmonic Generation Technique. *Spectrochim. Acta* **2001**, *57A*, 1417−1426 and references therein..
(52) Sowmiya, M.; Tiwari, A. K.; Saha, S. K. Study on intramolecular charge transfer fluorescence properties of *trans*-4-[4′-(*N*,*N*′-dimethylamino)styryl]pyridine: Effect of solvent and pH. *J. Photochem. Photobiol. A: Chem.* **2011**, *218*, 76−86.
(53) Sonu; Tiwari, A. K.; Sarmah, A.; Roy, R. K.; Saha, S. K. Study on photophysical properties and prototropic equilibria of *trans*-2-[4-(*N*,*N*-dimethylaminostyryl)]pyridine. *Dyes Pigm.* **2014**, *102*, 114−125.
(54) Shizuka, H. Excited-State Proton-Transfer Reactions and Proton-Induced Quenching of Aromatic Compounds. *Acc. Chem. Res.* **1985**, *18*, 141−147.
(55) Arnaut, L. G.; Formosinho, S. J. Excited-state proton transfer reactions I. Fundamentals and intermolecular reactions. *J. Photochem. Photobiol. A: Chem.* **1993**, *75*, 1−20.
(56) Tolbert, L. M.; Solntsev, K. M. Excited-State Proton Transfer: From Constrained Systems to "Super" Photoacids to Superfast Proton Transfer. *Acc. Chem. Res.* **2002**, *35*, 19−27.
(57) Lewis, F. D.; Sinks, L. F.; Weigel, W.; Sajimon, M. C.; Crompton, E. M. Ultrafast Proton Transfer Dynamics of Hydroxystilbene Photoacids. *J. Phys. Chem. A* **2005**, *109*, 2443−2451.
(58) Presiado, I.; Karton-Lifshin, N.; Gepshtein, R.; Shabat, D.; Huppert, D. Ultrafast Proton Transfer of Three Novel Quinone Cyanine Photoacids. *J. Phys. Chem. A* **2012**, *116*, 7353−7363.
(59) Perrin, D. D. *Dissociation Constants of Organic Bases in Aqueous Solution*; Butterworths: London, 1965.
(60) Sowmiya, M.; Sonu; Tiwari, A. K.; Saha, S. K. Study on intramolecular charge transfer fluorescence properties of *trans*-4-[4′-(*N*,*N*′-dimethylamino)styryl]pyridine: Effect of solvent and pH. *J. Photochem. Photobiol. A: Chem.* **2011**, *218*, 76−86.
(61) Abdel-Halim, S. T. Steady-state fluorescence and photoisomerization study of 1-methyl-4′-(*p*-*N*,*N*-dimethyl-amino styryl) pyridinium iodide. *J. Lumin.* **2011**, *131*, 30−35.


DOI: 10.1021/jp510982h
*J. Phys. Chem. A* XXXX, XXX, XXX−XXX